JOURNAL OF BACTERIOLOGY, July 1983, p. 381–390
0021-9193/83/070381-10$02.00/0

Vol. 155, No. 1

Electron Microscopy of Frozen-Hydrated Bacteria

JACQUES DUBOCHET,[1]* ALASDAIR W. McDOWALL,[1] BEATE MENGE,[2] ERNST N. SCHMID,[2] AND KARL G. LICKFELD[2]

European Molecular Biology Laboratory, D-6900 Heidelberg,[1] and Institut für Medizinische Mikrobiologie, Klinikum der Universität Essen GHS, D-4300 Essen,[2] Federal Republic of Germany

Received 18 February 1983/Accepted 30 April 1983

Amorphous, unstained, frozen-hydrated sections of bacteria provide a faithful high-resolution image of procaryotic cells. Conventional preparation artifacts due to fixation, staining, and dehydration are nonexistent. Freezing damage is avoided by using glucose as a cryoprotectant. Cutting damage on frozen material is severe, but sectioning artifacts, being always related to the cutting direction, can be systematically recognized and thus taken into consideration. Geometry and density distribution of the bacterial envelope can be resolved to about 3 nm. The following main features have been observed. In *Escherichia coli* the inner and outer membranes have an approximately uniform density profile. The distance between the two membranes is constant, ca. 33 nm. In *Staphylococcus aureus* the cell wall is ca. 40 nm wide. It is bordered on the cytoplasmic side by an asymmetric 5.5-nm-wide bilayer. The bacterial nucleoid, clearly visible with conventional preparation methods, appears in exponentially growing bacteria as an ill-defined central region with approximately the same density as the rest of the cytoplasm. It becomes more clearly visible when bacteria are in the stationary phase, plasmolysed, fixed, or stained. We confirm that "mesosomes," hitherto quite often considered to be essential organelles in all procaryotes, are artifacts. They appear in large numbers during osmium fixation.

Conventional specimen preparation methods for electron microscopy involve steps which are artifact prone. It is widely believed that chemical fixation, staining, and replacement of water by dehydrating agents and resins are particularly harmful to biological structures. Continuing a long effort in cryoelectron microscopy (20), the recent development of a method for high-resolution observation of sectioned, frozen-hydrated biological material overcomes these artifacts (J.-J. Chang, A. W. McDowall, J. Lepault, R. Freeman, C. A. Walter, and J. Dubochet, J. Microsc., in press; A. W. McDowall, J.-J. Chang, R. Freeman, J. Lepault, C. A. Walter, and J. Dubochet, J. Microsc., in press). For the first biological application of the new method, we studied how the structures of some typical gram-positive and gram-negative bacteria appear in frozen-hydrated sections. In particular we focused our attention on the fine structure of the bacterial envelope and addressed the question of whether the confined bacterial nucleoid and mesosomes are naturally occurring procaryotic structures or artifacts of conventional preparation techniques.

(This work is being submitted in part by A.W.M. for the Fellowship Thesis of the Institute of Medical Laboratory Sciences [Institute of Medical Laboratory Sciences, London].)

MATERIALS AND METHODS

Bacteria. *Bacillus subtilis* (clinical isolate), *Escherichia coli* ATCC 11775, *Klebsiella pneumoniae* biovar d, and *Staphylococcus aureus* ATCC 12600 were grown in LB broth (13) with 10 to 15% glucose (0.6 to 0.9 M) added as a cryoprotectant. *E. coli* cells were harvested at a concentration of 5×10^7 CFU/ml while growing in exponential phase and 10^9 to 10^{10} CFU/ml in stationary phase. *S. aureus* cells in exponential growth phase were harvested at 3×10^8 CFU/ml.

Preparation for electron microscopy. The general procedure for the preparation and observation of frozen-hydrated specimens has been described previously (McDowall et al., in press). The bacteria in their growing medium are pelleted by centrifugation at $12{,}000 \times g$ for 15 s. A ca. 10-μg fraction of the pellet is applied to the 0.3-mm-diameter flat surface of a microtome specimen holder and immediately projected into liquid ethane. The total time for this maneuver is less than 30 s; the exposure of the pellet to air before freezing is less than 1 s. After freezing, the specimen is retained under liquid nitrogen until required.

The specimens are sectioned with a diamond knife in an FC-4 cryoultramicrotome (Reichert-Jung) operating at 120 K. Individual sections or groups of sections are transferred at low temperature onto a carbon-coated 700-hexagonal-mesh supporting grid, where they are pressed between two polished copper surfaces. The transfer from the copper block to a cold-stage PW 6591/100 of a Philips 400 electron microscope takes place under liquid nitrogen. The specimen is immediately introduced into the microscope. It has

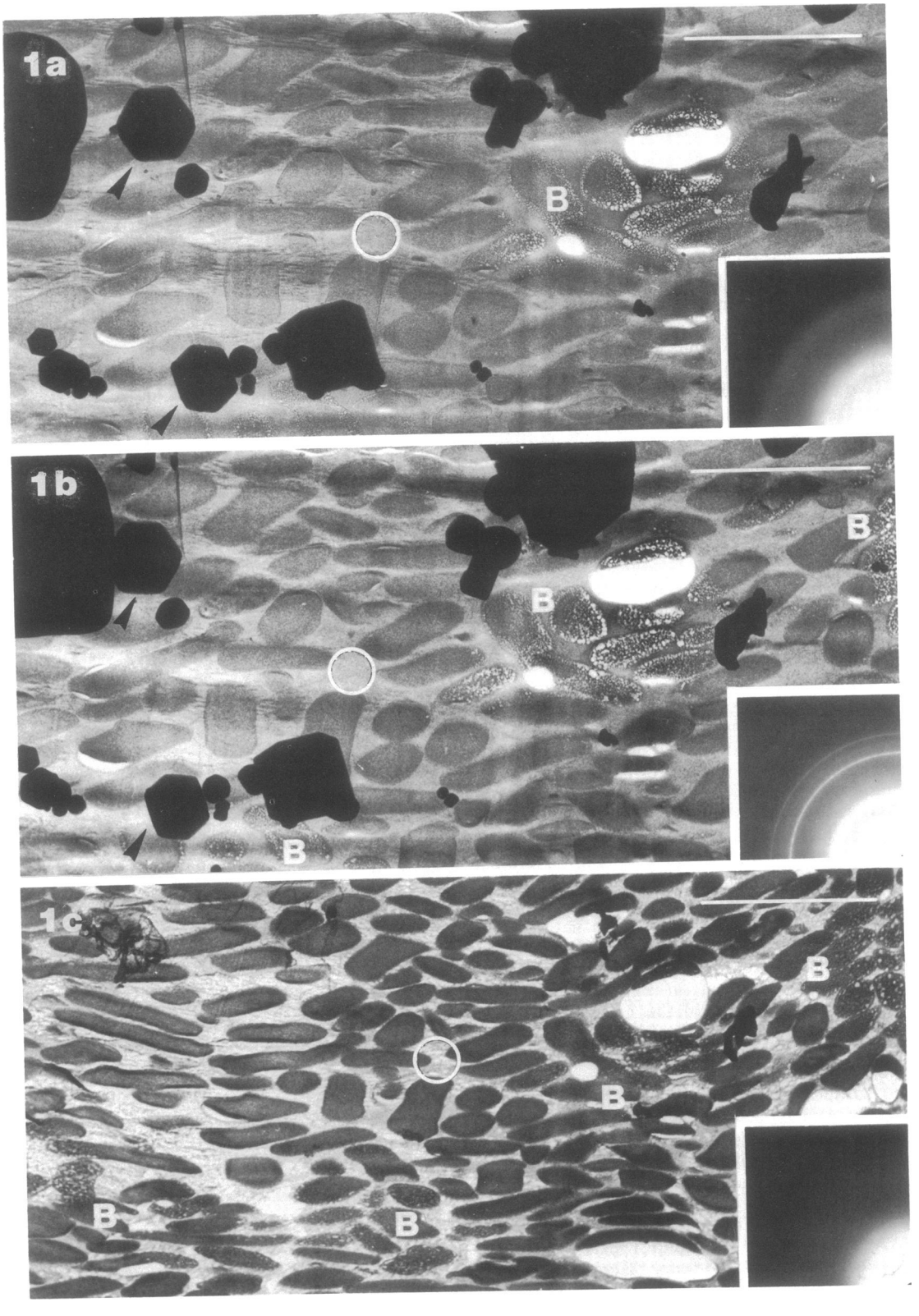
1a
B
1b
B
B
B
1c
B
B
B
B

been demonstrated previously (8) that the transfer is made without raising the section temperature above 135 K and without severe contamination by ice crystals or condensed amorphous solid water.

Control samples were prepared by the conventional procedure involving osmium fixation (19) and Epon embedding.

Observation. Frozen-hydrated specimens were observed at around 110 K in a Philips 400 electron microscope operating at 80 kV in the bright-field imaging or electron diffraction mode. The images were recorded at magnifications not larger than 20,000 times on Kodak Electron Image Film SO 163 developed for 4 min in full-strength D19 Kodak developer. Unless otherwise stated, the total irradiation of the specimen was less than 1,000 electrons per nm^2. After observation at low temperature, the specimens were warmed up in the electron microscope (approximate rate at 160 K, 10 K min^{-1}). Crystallization and freeze-drying were observed during warming.

Mass thickness and density values from one point on the section were calculated on the basis of optical density readings made on the negative (10). The mass thickness ρt is given by the equation:

$$\rho t = \lambda \ln D_0/D_1 \quad (1)$$

in which ρ is the density (grams per cubic centimeter), t is the thickness (nanometers), and D_0 and D_1 are, respectively, the optical density of the image of an empty region of the section (hole) and of one point on the section. All optical densities are measured above fog level. λ is the mean mass thickness which, under the conditions used in this study, has a value of 200 mg m^{-2}. Equation 1 holds with the following assumptions. (i) The optical density above the fog level is proportional to the electron dose. For the photographic film used in this study this hypothesis holds to within 5% up to an optical density of 1.5 U. (ii) The number of electrons scattered in a volume element is proportional to the density of the material. According to theoretical calculations, this hypothesis holds to within 3% for the various constituents of biological material.

The density ρ at one point of the section is given by the equation:

$$\rho = \rho_s[\ln(D_0/D_2)]/[\ln(D_0/D_1)] \quad (2)$$

where ρ_s is the density of the solute and D_0, D_1, and D_2 are, respectively, the optical density of the image of an empty region of the section, of the frozen solution (interspace between bacterial), and of the biological material. Equation 2 holds with the following additional assumption: (iii) the thickness of the section is constant over the region where D_1 and D_2 are measured. Furthermore, (iv) the density of the solution (as measured between the bacteria) is arbitrarily given the value of 1 g cm^{-3}. This normalization is acceptable insofar as the relative density between solution and biological structure is independent of the presence of sugar or other ingredients of the growth medium and is unaffected by freezing. If this is the case, our measure of ρ represents the density in a dilute liquid growing medium without sugar.

Optical-density measurements were made in white light with a Joyce-Loebel 3CS optical microdensitometer.

RESULTS

Sections. Sections clearly showing biological structures can easily and reproducibly be obtained on amorphous frozen-hydrated samples. If, however, water crystallizes during freezing, obtaining thin sections is extremely difficult and biological structures are severely damaged. In this study, only amorphous frozen-hydrated sections were considered.

Amorphous frozen-hydrated sections have an electron diffractogram characterized by two broad rings situated at 2.7 and 4.7 nm^{-1}, respectively, with a half-width of approximately 0.3 nm^{-1} (Fig. 1a). Upon warming, frozen water of the section transforms at around 145 K into cubic ice, characterized by three sharp rings situated at 2.73, 4.46, and 5.21 nm^{-1} (Fig. 1b). Further warming causes most of the water to evaporate during the temperature rise from 175 to 185 K. During freeze-drying, the mass thickness of the section decreases and the contrast of the biological material increases. In most cases, the section shrinks considerably, and rearrangement of the residual material causes the loss of fine detail (Fig. 1c). Comparing the mass thickness of the section before and after freeze-drying allows determination of the proportion of water originally contained in the sample. For this calculation the shrinkage of the section during freeze-drying must be compensated for by multiplying the mass thickness of the section by the inverse square of the linear shrinkage ratio. In the case of the specimen shown in Fig. 1, the linear shrinkage ratio was 0.63 and the dry mass

FIG. 1. Transformation upon warming of an amorphous frozen-hydrated section of *E. coli* in 15% glucose. The three images of the same region have been recorded and printed under the same conditions to show the contrast variation that takes place during freeze-drying. Corresponding electron diffractograms recorded from a different but similar series are shown in inserts. The scale is given by the middle sharp ring of cubic ice [insert in (b)] corresponding to 4.46 nm^{-1}. Contaminating ice crystals are marked by arrowheads. Regions where bubbling has taken place while the beam was concentrated on this area are designated B. A typical region used for hydration measurement is circled. Initial thickness of the section was 140 nm. Temperature: (a) 120 K; (b) 155 K; (c) 210 K. Bars, 3 μm.

thickness in the interspace between bacteria was 17 ± 4% of the mass thickness of the hydrated sample.

The process of sectioning causes damage to the sample. Besides folds, tears, chatter, and knife marks, which are also common (though less pronounced) in plastic sections, the following cutting-induced artifacts are characteristic for frozen-hydrated sections.

(i) Sections suffer from a compression along the cutting direction. The phenomenon, which also takes place in plastic sections (17), is much more severe in frozen-hydrated sections. As measured from the average ellipticity of *S. aureus* (see Fig. 9), dimensions along the cutting direction are reduced by 30 to 50%.

(ii) Crevasses, clearly visible, for example, in the region marked C in Fig. 2 and in the interspace between bacteria in Fig. 9, are characterized by irregular, densely packed fractures roughly parallel to the cutting edge. They appear in a minority of amorphous sections and in general are limited to those regions with a lower concentration of biological material.

(iii) Local distortions or fractures frequently take place in regions with abrupt changes in

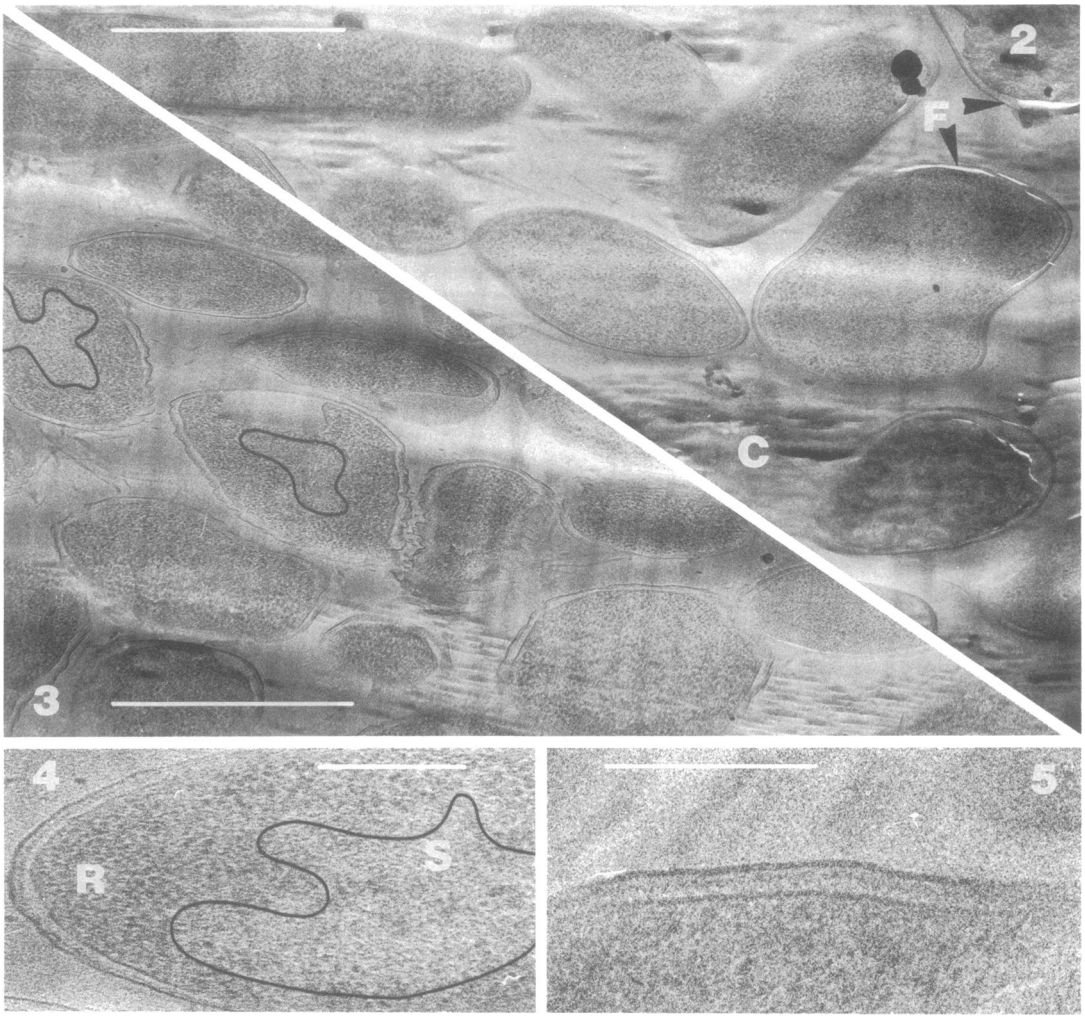

FIG. 2. Amorphous frozen-hydrated section of *E. coli* harvested while growing in exponential phase. A region with crevasses is marked C. Fractures along the cell membranes are marked F. Bar, 1 μm.

FIG. 3. Same material as in Fig. 2, but harvested in stationary phase. For two bacteria, the smooth central region has been delineated. Bar, 1 μm.

FIG. 4. Enlarged view of Fig. 2 showing the smooth (S) central and rough (R) external regions of the *E. coli* cytoplasm. A tentative borderline has been drawn between these two regions. Bar, 0.2 μm.

FIG. 5. Enlarged view of Fig. 2 showing the typical aspect of the *E. coli* cell envelope. Bar, 0.2 μm.

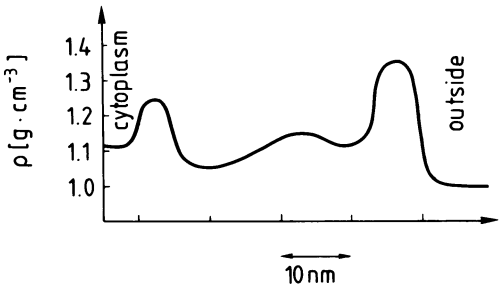

FIG. 6. Average density profile of *E. coli* envelope.

density. This can be seen, for example, in Fig. 2, where two fractures (F) associated with the cell envelope are marked, and in Fig. 9, where the bacteria appear asymmetric in respect to the knife direction, one side appearing sharper than the other. In the same micrograph, the bacterial envelope at the region of sharper curvature frequently seems to be divided into two adjacent, wedge-shaped layers, as is the case in the circled region.

Frozen-hydrated sections are beam sensitive. The damage appears initially as bubbling (8), starting at around 2,000 electrons per nm^2. This threshold dose for bubbling decreases with increasing concentration of biological material.

Gram-negative bacteria: *E. coli* and *K. pneumoniae*. The general aspect of a sectioned bacterial pellet is shown in Fig. 2 and 3 for *E. coli*. Sectioned *K. pneumoniae* pellets have a similar appearance (not shown). In Fig. 2, the bacteria are in exponential growth phase, whereas In Fig. 3 they are from a stationary culture. Bacteria are clearly visible and are sharply delineated by the bacterial envelope. Flagella and pili can be seen in the interspaces between cells. The average density inside *E. coli* is 1.11 ± 0.04 g cm^{-3}. As shown in Fig. 4 (enlarged view of Fig. 2), the cytoplasm exhibits two kinds of structures: (i) the nucleoid, a smooth region with sometimes filamentous appearance in the center of the bacterium, and (ii) the coarse peripheral cytoplasm with ribosomes, which lie individually or arranged in short rows. In exponentially growing bacteria there is no measurable density difference between these two regions. They are separated by an irregular transition zone (Fig. 4). The differentiation of the two regions of the cytoplasm is enhanced when bacteria are in stationary phase (Fig. 3) and even more when they are plasmolysed, chemically fixed, or stained (see Fig. 7).

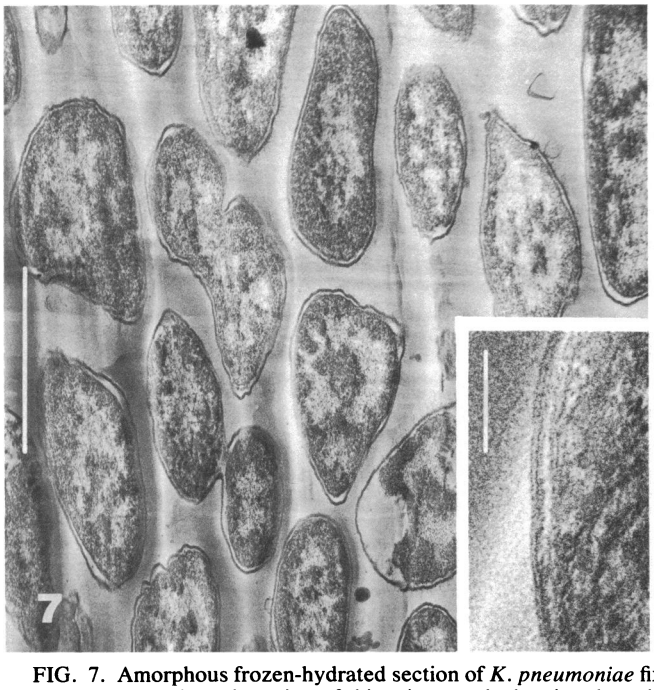

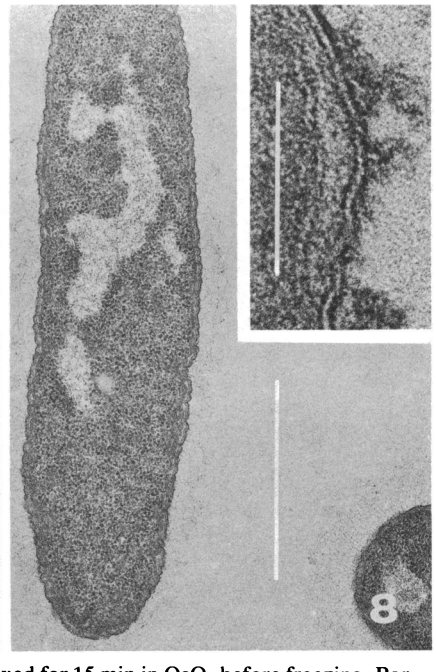

FIG. 7. Amorphous frozen-hydrated section of *K. pneumoniae* fixed for 15 min in OsO_4 before freezing. Bar, 1 μm. (Insert) Enlarged portion of this micrograph showing the cell wall. Bar, 0.1 μm.

FIG. 8. Conventionally prepared specimen of *K. pneumoniae* (OsO_4 fixation; Epon embedding; poststaining with lead citrate; observed at room temperature). (Insert) Typical aspect of conventionally prepared cell wall (*E. coli*). Bar, 0.1 μm.

The envelope of *E. coli* has a characteristic aspect (Fig. 5). The average density profile deduced from 12 measurements is drawn in Fig. 6. The sharply defined outer membrane approximates to a rectangular profile with a density of 1.35 ± 0.07 g cm^{-3}. Its width at half height is 7 ± 1 nm. The inner membrane has a more Gaussian profile (5 ± 1 nm wide) with a maximal density of 1.25 ± 0.07 g cm^{-3}. The center-to-center distance between inner and outer membranes is 39 nm. This distance seems to be very constant, even though our measurements may be imprecise due to the compression of the section. A faint, 8-nm-wide line (measured at half height; Fig. 6), with a density of 1.15 in the center, occupies a part of the space between inner and outer membranes. The periplasmic space close to the inner membrane has a density of 1.05 g cm^{-3}. This space becomes irregular when bacteria are not exponentially growing, when they are

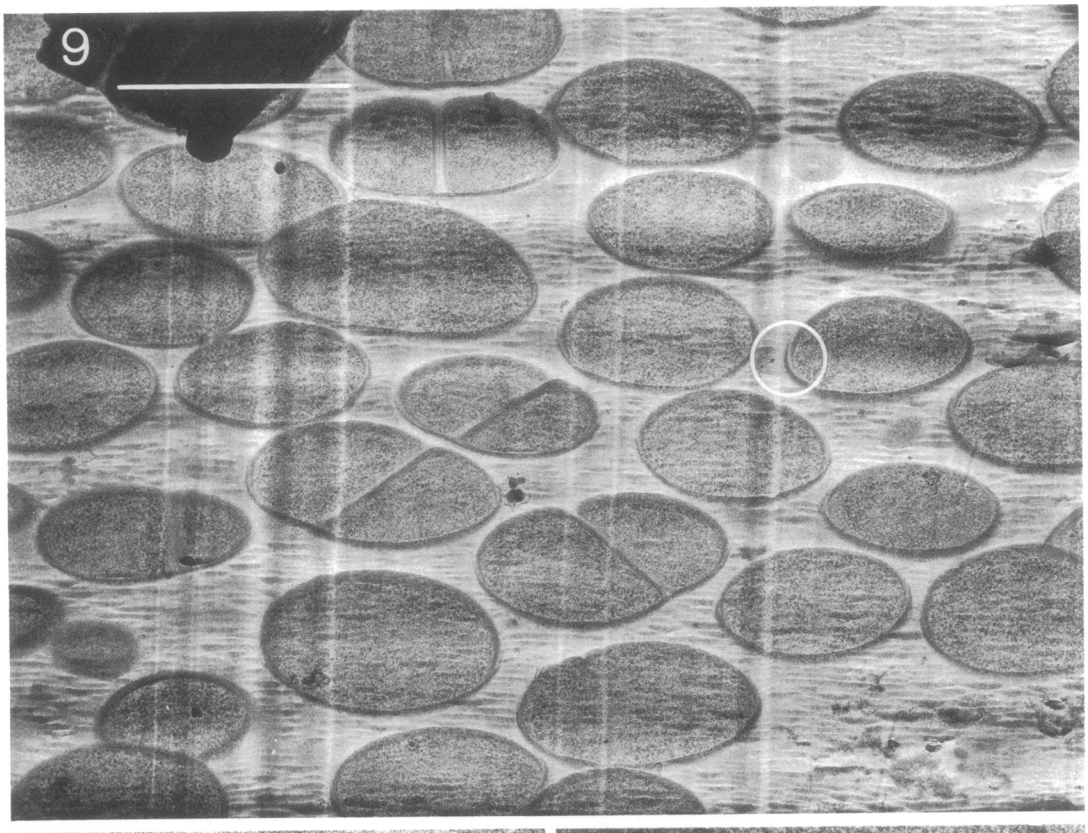

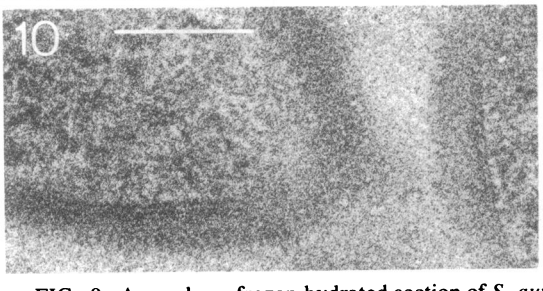

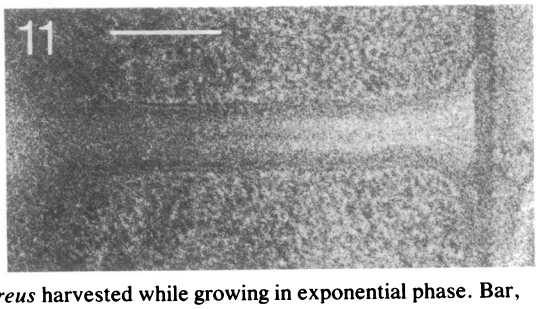

FIG. 9. Amorphous frozen-hydrated section of *S. aureus* harvested while growing in exponential phase. Bar, 1 μm. Circled area marks a typical cutting artifact.

FIG. 10. Enlarged view of the same sample as the one shown in Fig. 9. The envelope and part of the cytoplasm of two neighboring bacteria are visible. Bar, 0.1 μm.

FIG. 11. Septum of *S. aureus*. Enlarged view of Fig. 9. Bar, 0.1 μm.

in close contact with each other, or when they are plasmolysed, and also after fixation or staining.

The structure and mass distribution of *K. pneumoniae* cells fixed with osmium tetroxide before being frozen (Fig. 7) are very different from those of unfixed, frozen cells. A nucleoid region of low density is visible in most bacteria, as is also the case in conventionally embedded preparations (Fig. 8). The nucleoid frequently is filamentous, probably due to aggregated DNA strands. The cytoplasmic region between envelope and nucleoid is dense (1.5 to 2.2 g cm^{-3}), demonstrating that it contains a large amount of stain. The cell envelope of the fixed, frozen bacteria is similar to the envelope seen in conventionally embedded bacteria. The outer and inner membranes have the characteristic "unit membrane" aspect (Fig. 7 and 8, inserts).

Gram-positive bacteria: *B. subtilis* and *S. aureus*. The general appearance of a sectioned bacterial pellet of exponential-phase *S. aureus* cells is shown in Fig. 9. *B. subtilis* appears similar (not shown). The average density inside *S. aureus* is 1.16 ± 0.04 g cm^{-3}. As is the case for gram-negative bacteria, a smooth central nucleoid is surrounded by a more granulated zone. In exponential growth-phase bacteria, the two regions have the same density. No mesosomes or any similar structures have been observed in unfixed frozen preparations.

The ca. 40-nm-thick envelope of *S. aureus* appears as shown in Fig. 9 and 10. The real width and density profile of the gram-positive envelope are still uncertain due to the warping effect of the sectioning process. A density profile, deduced from 12 measurements on regions of relatively good preservation, is given in Fig. 12. On the cytoplasmic side, the density profile is characterized by an asymmetric double layer of dense material 5.5 ± 1 nm wide.

Septa in dividing *S. aureus* are shown in Fig. 9. An enlarged view is given in Fig. 11, and the density profile for the septum is shown in Fig. 13. As is the case for the cell envelope, the septum is characterized by a 5.5-nm-wide, asymmetric double layer on the cytoplasmic side. The density distribution through the septum depends on the growth phase of the bacterium. The high-density layer in the medial plane is also observed by conventional thin-sectioning techniques.

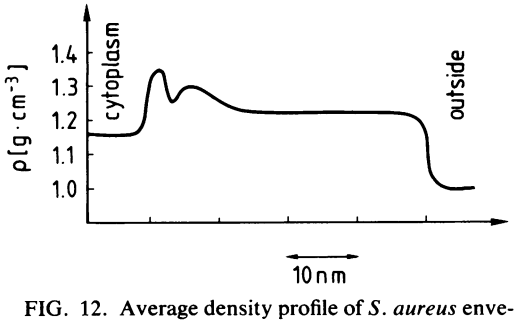

FIG. 12. Average density profile of *S. aureus* envelope.

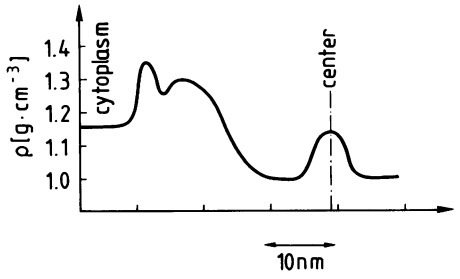

FIG. 13. Density profile of the septum shown in Fig. 11.

After fixation with OsO_4 and freezing, gram-positive bacteria are characterized by conspicuous nucleoids with filamentous structures and membranous mesosomes (N and M, respectively, in Fig. 14, which shows *S. aureus* cells fixed overnight). These bacteria are similar to those observed in conventionally embedded specimens (Fig. 14, insert). Fixation for 15 min causes a similar condensation of the nucleoid and also induces the formation of mesosomes, though smaller and less numerous. The density profile of the envelope is not uniform, and a low-density gap appears on its cytoplasmic border. The double layer visible in unfixed frozen specimens cannot be seen.

DISCUSSION

Unstained, amorphous, frozen-hydrated sections provide a faithful, high-resolution representation of living material. This statement is correct if we accept (i) that the bacteria have not been damaged during growth in the presence of glucose and during the short harvesting process, (ii) that we have demonstrated that the original hydration of the biological material is really preserved in the sections, and (iii) that either the sections are free of artifacts or the artifacts can be circumvented. With the preparation method used in this study, chemical fixation and staining artifacts do not exist. The possible sources of damage are therefore only freezing, sectioning, and irradiation.

That the original hydration of the bacterial pellet is preserved in the section was demonstrated by freeze-drying experiments which showed that the mass loss during freeze-drying was as expected for fully hydrated specimens. The possibility that after the section has been

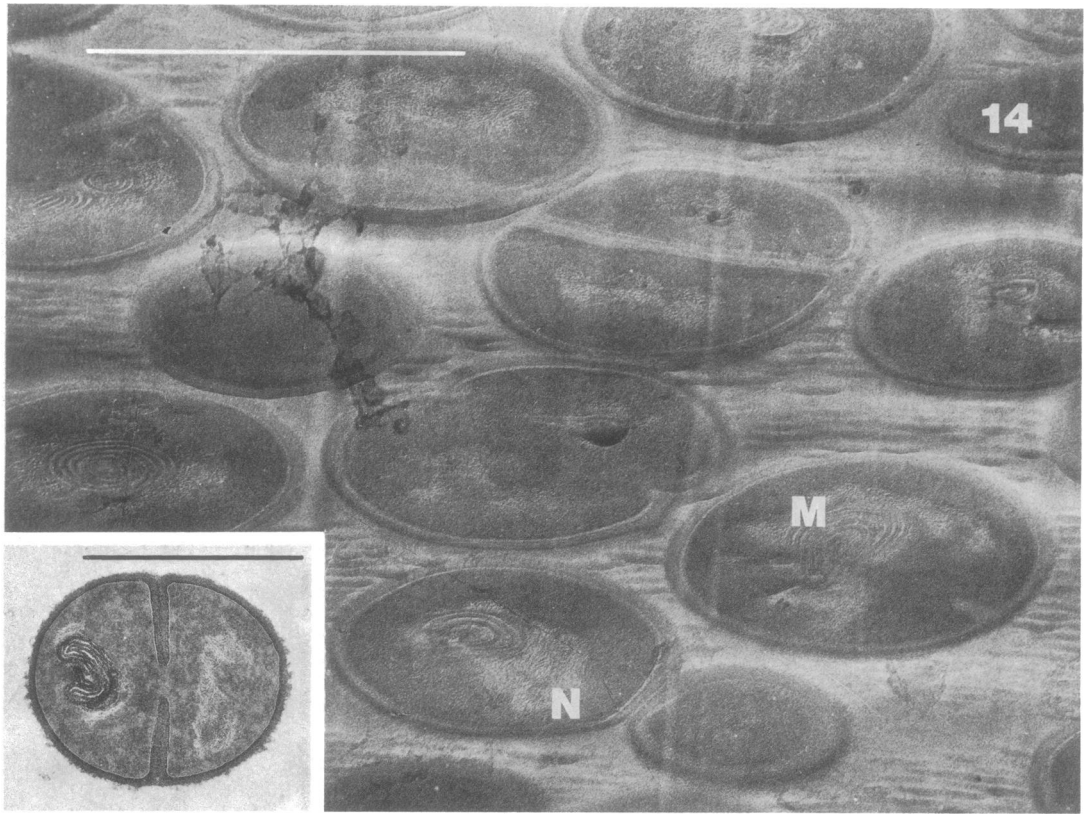

FIG. 14. Amorphous frozen-hydrated section of *S. aureus* fixed overnight in 1% OsO_4 before freezing. Nucleoids and mesosomes are marked by N and M, respectively. A conventionally prepared *S. aureus* cell is shown in insert. Bar, 1 μm.

made the surface undergoes partial freeze-drying, sufficient to modify contrast although too small to be detected by hydration measurements, was ruled out for the following reason. Only amorphous frozen-hydrated sections were observed in this study. Since crystallization of amorphous dilute solutions is an irreversible process which takes place within minutes at around 145 K, we know that our specimens were not warmed above this temperature before observation. On the basis of the known evaporation rate of water as a function of the temperature, it can then be deduced that the maximum evaporated layer is in the range of 0.1 nm.

No trace of freezing damage was observed on amorphous frozen-hydrated sections. In particular, the sample was not divided into domains of pure ice or concentrated biological material. This is not surprising since the crystalline order of water in amorphous samples, judged from the half-width of the diffraction rings, does not exceed 3 nm. Whether the molecular structure of the liquid is also preserved in the amorphous sample is presently a matter of debate (12) which is outside the scope of this study.

Apart from irradiation damage, sectioning is the only source of artifacts which can clearly be recognized on amorphous frozen-hydrated sections, as discussed previously (Chang et al., in press). Such artifacts all have in common the property of being related to the cutting direction. Consequently, sectioning artifacts can surely be recognized as such, in contrast to those due to fixation and dehydration which are encountered in conventionally prepared specimens.

The observation of unstained frozen-hydrated specimens provides a unique method for the measurement of density. In principle, determination can be made down to the resolution of the image. Controls made previously on model specimens have shown that this method is precise (7). When measurements are made on sections, the main source of error is probably the nonuniform thickness of the section. The use of a scanning transmission electron microscope will make density mapping more accurate and more rapid and, when the apparatus is used in the Z-contrast mode of image formation (6), should allow observers to eliminate errors due to surface irregularities.

The resolution at which biological observations can be made on sections of conventionally embedded specimens is generally limited by preparation damage (fixation, staining, embedding). In amorphous frozen-hydrated sections, since most of this damage is suppressed, the resolution limit is set by the low contrast of unstained biological structures and by electron beam damage. The contrast limit is overcome in favorable cases: for example, when membranes span most or all of the section thickness. Structure details which would be very difficult to see with conventional methods can thus be observed. This is exemplified by the 5.5-nm-wide double layer visible on the cytoplasmic side of the gram-positive cell envelope. Judging by the sharpness of the density profile tracing, the significant resolution on well-defined structures is less than 3 nm.

Our observations on the division of the cytoplasm into two structurally different regions support the concept that in procaryotic cells the DNA is localized in a confined area. The classical image of a well-confined, filamentous nucleoid observed in conventionally embedded samples (16) is exaggerated, however. The fact that the density in the two regions is the same, and that they have an ill-defined transition, explains the finding that a distinct DNA region cannot be demonstrated by freeze-fracturing unless chemically fixed cells are used (15, 18).

So-called mesosomes (11) do not exist in exponentially growing *S. aureus* bacteria. We confirm that they are fixation artifacts generated immediately after the onset of fixation (1, 5, 9, 18; A. Ryter, personal communication).

Conventionally prepared membranes always have the characteristic three-layer "unit-membrane" configuration, which is sometimes interpreted as representing the two hydrophilic surfaces of the membrane separated by the hydrocarbon tails of the lipids bilayer. More probably, the three-layer configuration results from nonspecific heavy metal deposition on the denatured surfaces of the membrane (14). Our observations of unfixed, unstained frozen-hydrated bacterial membranes show that each type of membrane has its typical fine structure. The outer membrane of *E. coli* has a nearly rectangular density profile. The somewhat thinner inner membrane has a more bell-shaped profile. The very thin membrane observed on the cytoplasmic border of the cell wall of *S. aureus* appears as an asymmetric bilayer. We have shown in a previous study (McDowall et al., in press) that myelin sheaths present a further aspect, compatible with results obtained from X-ray studies. The fact that membranes which are known to be biochemically very different also appear with different structures is a favorable hint on the credibility of our observations. One can also note that the density profile of the outer membrane is compatible with the one obtained from three-dimensional reconstruction of porin crystalline layers (A. Engel, personal communication).

The space between inner and outer membranes in *E. coli* has a uniform width. Our observations do not support the idea that there are many well-defined sites where inner and outer membranes come in close contact (2, 3). We would not, however, be able to observe such contacts if they were less than 20 to 30 nm wide.

Previous observations of the peptidoglycan of *E. coli* lead to a postulated 3.4-nm-thick layer with a density of 1.4 g cm^{-3} (4), directly attached to the outer membrane. The diffuse dense line we have observed between inner and outer membrane (Fig. 5 and 6) does not fit well with this description. More work needs to be done on the biochemical nature of this layer.

ACKNOWLEDGMENTS

We thank E. Kellenberger and A. Ryter for advice and unpublished information.

LITERATURE CITED

1. **Achterrath, M., and K. G. Lickfeld.** 1972. Number, size and location of *Staphylococcus* mesosomes—a function of fixation parameters, p. 220–221. *In* Proceedings of the Fifth European Congress on Electron Microscopy, Manchester. Institute of Physics, London.
2. **Bayer, M. E.** 1975. Role of adhesion zones in bacterial cell-surface function and biogenesis, p. 393–427. *In* A. Tzagoloff (ed.), Membrane biogenesis. Plenum Publishing Corp., New York.
3. **Bayer, M. H., G. P. Costello, and M. E. Bayer.** 1982. Isolation and partial characterization of membrane vesicles carrying markers of the membrane adhesion sites. J. Bacteriol. **149**:758–767.
4. **Beveridge, T. J.** 1981. Ultrastructure, chemistry and function of the bacterial wall. Int. Rev. Cytol. **72**:229–317.
5. **Burdett, I. D. J., and H. J. Rogers.** 1970. Modification of the appearance of mesosomes in sections of *Bacillus licheniformis* according to the fixation procedures. J. Ultrastruct. Res. **30**:354–367.
6. **Carlemalm, E., and E. Kellenberger.** 1982. The reproducible observation of unstained embedded cellular material in thin sections: visualization of an integral membrane protein by a new mode of imaging for STEM. EMBO J. **1**:63–67.
7. **Dubochet, J., J.-J. Chang, R. Freeman, J. Lepault, and A. W. McDowall.** 1982. Frozen aqueous suspensions. Ultramicroscopy **10**:55–62.
8. **Dubochet, J., J. Lepault, R. Freeman, J. A. Berriman, and J.-C. Homo.** 1982. Electron microscopy of frozen water and aqueous solutions. J. Microsc. **128**:219–237.
9. **Ebersold, H. R., J.-L. Cordier, and P. Lüthy.** 1981. Bacterial mesosomes: method dependent artefacts. Arch. Microbiol. **130**:19–22.
10. **Eusemann, R., H. Rose, and J. Dubochet.** 1982. Electron scattering in ice and organic materials. J. Microsc. **128**:239–249.
11. **Fooke-Achterrath, M., K. G. Lickfeld, V. M. Reusch, U. Aebi, U. Tschöpe, and B. Menge.** 1974. Close-to-life preservation of *Staphylococcus aureus* mesosomes for transmission electron microscopy. J. Ultrastruct. Res. **49**:270–285.

12. **Franks, F. (ed.).** 1982. Water. A comprehensive treatise, vol. 7. Plenum Publishing Corp., New York.
13. **Hohn, B., and T. Hohn.** 1974. Activity of empty, headlike particles for packaging of lambda DNA in vitro. Proc. Natl. Acad. Sci. U.S.A. **71**:2372–2376.
14. **Kellenberger, E., and J. Kistler.** 1979. The physics of specimen preparation, p. 49–79. *In* W. Hoppe and R. Mason (ed.), Advances in structure research, vol. VII. Vieweg & Sohn, Wiesbaden.
15. **Lickfeld, K. G.** 1968. Der frostgeätzte Bakterienkern. Ein Beitrag zur Klärung seiner Tertiärstruktur. Z. Zellforsch. **88**:560–564.
16. **Lickfeld, K. G., M. Achterrath, F. Hentrich, L. Kolehmainen-Seveus, and A. Persson.** 1972. Die Feinstrukturen von *Pseudomonas aeruginosa* in ihrer Deutung durch die Gefrierätztechnik, Ultramikrotomie und Kryo-Ultramikrotomie. J. Ultrastruct. Res. **38**:27–45.
17. **Lickfeld, K. G., B. Menge, H. Wunderli, J. van den Broek, and E. Kellenberger.** 1977. The interpretation and quantitation of sliced intracellular bacteriophages and phage-related particles. J. Ultrastruct. Res. **60**:148–168.
18. **Nanninga, N.** 1973. Freeze-fracturing of microorganisms: physical and chemical fixation of *Bacillus subtilis*, p. 151–180. *In* L. Benedetti and P. Favard (ed.), Freeze-etching, techniques and applications. Société Française de Microscopie Electronique, Paris.
19. **Ryter, A., E. Kellenberger, A. Birch-Anderson, and O. Maaløe.** 1958. Etude au microscope électronique de plasma contenant de l'acide désoxyribonucléique. Les nucléoides des bactéries en croissance active. Z. Naturforsch. **13b**:597–605.
20. **Somlyo, A. V., H. Gonzalez-Serratos, H. Shuman, G. McClellan, and A. P. Somlyo.** 1981. Calcium release and ionic changes in the sarcoplasmic reticulum of tetanized muscle: an electron probe study. J. Cell Biol. **90**:577–594.